Magnetic excitations in the spin-$\frac{1}{2}$ tetramer substance $Cu_2{}^{114}Cd^{11}B_2O_6$ obtained by inelastic neutron scattering experiments

Masashi Hase,[1,*] Kenji Nakajima,[2] Seiko Ohira-Kawamura,[2] Yukinobu Kawakita,[2]
Tatsuya Kikuchi,[2] and Masashige Matsumoto[3]
[1]*National Institute for Materials Science (NIMS), Tsukuba, Ibaraki 305-0047, Japan*
[2]*J-PARC Center, Tokai, Ibaraki 319-1195, Japan*
[3]*Department of Physics, Shizuoka University, Shizuoka 422-8529, Japan*
(Received 27 April 2015; published 16 November 2015)

We performed inelastic neutron scattering experiments on $Cu_2{}^{114}Cd^{11}B_2O_6$ powder. The magnetic excitations at low temperatures are similar to those of the interacting spin-$\frac{1}{2}$ tetramers in the ordered state. The weak excitations existing above 3 meV suggest that the Higgs mode appears in $Cu_2CdB_2O_6$ at ambient pressure and zero magnetic field. We evaluated $J_1 = 27.3 \pm 1.0$ and $J_2 = -14.0 \pm 1.4$ meV for the intratetramer interactions and $J_3 = -0.4 \pm 0.2$ and $J_4 = 1.4 \pm 0.2$ meV for the intertetramer interactions. The spin gap in the isolated spin tetramer was calculated to be 1.6 meV, which is less than the effective intertetramer interaction value (3.6 ± 0.8 meV). Therefore, antiferromagnetic long-range order is possible, although the ground state of the isolated spin tetramer is the spin-singlet state. We discuss the temperature dependence of the magnetic excitations.

DOI: 10.1103/PhysRevB.92.184412 PACS number(s): 75.10.Jm, 75.40.Gb, 75.30.Ds

I. INTRODUCTION

Antiferromagnetic (AF) XXZ models describe the competition between spin-singlet pairs and AF long-range order (AF-LRO). The Hamiltonian is expressed as

$$\mathcal{H} = \sum_{i,j} J_{ij}\left(\frac{S_{i+}S_{j-} + S_{i-}S_{j+}}{2} + \Delta S_{iz}S_{jz}\right). \quad (1)$$

The first term in the parentheses stabilizes spin-singlet pairs, induces quantum fluctuation, and destroys AF-LRO, whereas the second term stabilizes AF-LRO.

In spin-$\frac{1}{2}$ AF Heisenberg models ($\Delta = 1$) with nearest-neighbor exchange interactions, the dimensionality of the lattice affects the magnetism as follows. In a three-dimensional spin system on a simple cubic lattice, AF-LRO appears at finite temperatures. In a two-dimensional spin system on a square lattice, AF-LRO exists only at 0 K. The ground state (GS) is a combination of a Néel state and a resonating-valence-bond (RVB) state [1]. The magnitude of ordered magnetic moments is reduced by the overlap of the spin-singlet RVB state. In a one-dimensional spin system on a uniform chain, no AF-LRO exists even at 0 K. The GS is the gapless spin-singlet state known as a Tomonaga-Luttinger liquid (TLL). The spin correlation in a TLL decays algebraically. A TLL is a quasi-long-range-ordered state and is at quantum criticality. Therefore, infinitesimal interchain exchange interactions stabilize AF-LRO. Other perturbations such as the alternation of exchange interactions [2–4] and next-nearest-neighbor exchange interactions [5–7], on the other hand, generate a spin gap between the spin-singlet ground and first excited states and stabilize spin-singlet state(s).

In a zero-dimensional spin system on an isolated spin cluster, no AF-LRO exists even at 0 K. AF-LRO sometimes appears in weakly coupled spin clusters even when the GS of the isolated spin cluster is the spin-singlet state. We understand the mechanism of the appearance of AF-LRO to be as follows. The GS of weakly coupled spin clusters can be magnetic because of the following mechanism. The values of S^{T} and S_z^{T} are 0 in the spin-singlet GS. Here, S^{T} and S_z^{T} represent the value and z value, respectively, of the sum of the spin operators in a cluster. Other $S_z^{\mathrm{T}} = 0$ states can be hybridized with the spin-singlet GS of an isolated spin cluster by intercluster interactions [8]. States with $S^{\mathrm{T}} > 0$ and $S_z^{\mathrm{T}} = 0$ are magnetic. For example, S_z^{T} is zero in a collinear two-sublattice AF ordered state, although the state is not an eigenstate of AF Heisenberg models. As a result, the GS of weakly coupled spin clusters can become magnetic by the hybridization of plural $S_z^{\mathrm{T}} = 0$ states.

A gapless Nambu-Goldstone mode exists in AF-LRO because of broken symmetries [9]. Therefore, the excitation energy of a mode must be zero below the transition temperature T_{N}. Intercluster interactions change the discrete energy level of an isolated cluster to an energy band with a finite width. As the temperature T is lowered, the band width increases. If the spin gap is comparable to or less than the energy of the effective intercluster interaction, the gapless Nambu-Goldstone mode can appear and therefore AF-LRO can appear. Here, the effective intercluster interaction is given by the summation of the product of the absolute value of the intercluster interaction and the number of interactions per spin (z) [10].

There are several model substances with weakly coupled spin clusters showing AF-LRO. The spin system in $ACuCl_3$ ($A = NH_4$, K, or Tl) consists of coupled Cu-Cu dimers. These substances can have AF-LRO even at zero magnetic field. NH_4CuCl_3 exhibits AF-LRO at ambient pressure [11], whereas $KCuCl_3$ and $TlCuCl_3$ exhibit AF-LRO above critical pressures [12,13]. NH_4CuCl_3 has three types of dimers [14–16]. In one of them, the value of the intradimer interaction is 0.29 meV, which is less than the values of the effective interdimer interaction. Therefore, magnetic excitations generated by the dimer are gapless within the experimental accuracy [17]. The spin gap of $KCuCl_3$ is 2.60 meV, which is comparable to the value of the effective interdimer interaction [18]. The spin gap of $TlCuCl_3$ is 0.70 meV, which is less than the values of the effective interdimer interaction [18]. As the pressure is raised

*HASE.Masashi@nims.go.jp

or the temperature is lowered in $TlCuCl_3$, the triplet excitations are softened and become gapless at T_N [19,20]. In the ordered state, degenerate triplets are separated into transverse (Nambu-Goldstone) and longitudinal (Higgs) modes.

Several AF-LROs can be explained in the scheme of weakly coupled spin clusters. For example, if we consider that the spin system in $Cu_2Fe_2Ge_4O_{13}$ comprises weakly coupled Fe-Cu-Cu-Fe tetramers (four-spin systems) [10], we can more easily understand the ordering mechanism of magnetic moments on Cu^{2+} ions. The spin system was considered as a combination of spin-$\frac{1}{2}$ Cu dimers and spin-$\frac{5}{2}$ Fe chains [8,21–24]. The values of the intradimer and intrachain exchange interactions (J_{Cu} and J_{Fe}, respectively) are 22.0 and 1.60 meV, respectively. An exchange interaction ($J_{Cu\text{-}Fe}$) couples a dimer and chain, where the value of $J_{Cu\text{-}Fe}$ is 2.30 meV. The magnetic excitations corresponding to singlet-triplet excitations in Cu dimers have been observed around 24 meV [8]. In spite of the large value of J_{Cu}, which appears to stabilize a (nearly) spin-singlet state of Cu spins, both Cu and Fe moments are cooperatively ordered below $T_N = 39$ K. The magnitudes of Cu and Fe moments are 0.38(4) and 3.62(3) μ_B, respectively, where the Cu moments are not so small.

The Fe-Cu-Cu-Fe tetramer can be considered to be formed by the J_{Cu} and $J_{Cu\text{-}Fe}$ interactions. The GS of the isolated tetramer is the spin-singlet state. The spin gap in the isolated tetramer was calculated to be 0.11 meV in spite of the large values of the J_{Cu} and $J_{Cu\text{-}Fe}$ interactions. The spin gap is smaller than the value of the effective intercluster interaction. Accordingly, we can understand the appearance of the cooperative order in the scheme of weakly coupled spin clusters.

The mechanism of the appearance of AF-LRO below $T_N = 9.8$ K in $Cu_2CdB_2O_6$ [25,26] appears to be analogous to that in $Cu_2Fe_2Ge_4O_{13}$. We observed a $\frac{1}{2}$ quantum magnetization plateau above 23 T at 2.9 K. A quantum magnetization plateau does not appear in conventional AF-LROs and indicates the existence of an energy gap. From the magnetization results [25] and the magnetic structure [27], we have determined that the spin system in $Cu_2CdB_2O_6$ consists of weakly coupled spin-$\frac{1}{2}$ tetramers. Each tetramer is formed by the antiferromagnetic J_1 and ferromagnetic J_2 exchange interactions as shown in Fig. 1(a). The values of J_1 and J_2 were evaluated to be 264 K (22.7 meV) and -143 K (-12.3 meV) in the previous work [27]. The GS of the isolated tetramer is the spin-singlet state. The spin gap in the isolated tetramer was calculated to be 1.43 meV in spite of the large values of the J_1 and J_2 interactions. In the previous papers [25,27], we considered only the J_3 interaction ($z = 2$) as the intertetramer interaction. The $z|J_3|$ value was evaluated to be 9.9 K (0.85 meV), which is comparable to the spin gap. To investigate whether the AF-LRO in $Cu_2CdB_2O_6$ can be understood in the scheme of weakly coupled spin clusters, we performed inelastic neutron scattering (INS) experiments on $Cu_2{}^{114}Cd^{11}B_2O_6$ powder to obtain its magnetic excitations.

II. EXPERIMENTAL AND CALCULATION METHODS

Crystalline $Cu_2{}^{114}Cd^{11}B_2O_6$ powder was synthesized by a solid-state reaction at 1073 K in air for 160 h with intermediate grindings. We used the isotopes ^{114}Cd and ^{11}B to decrease the absorption of neutrons. The purity of the isotopes was

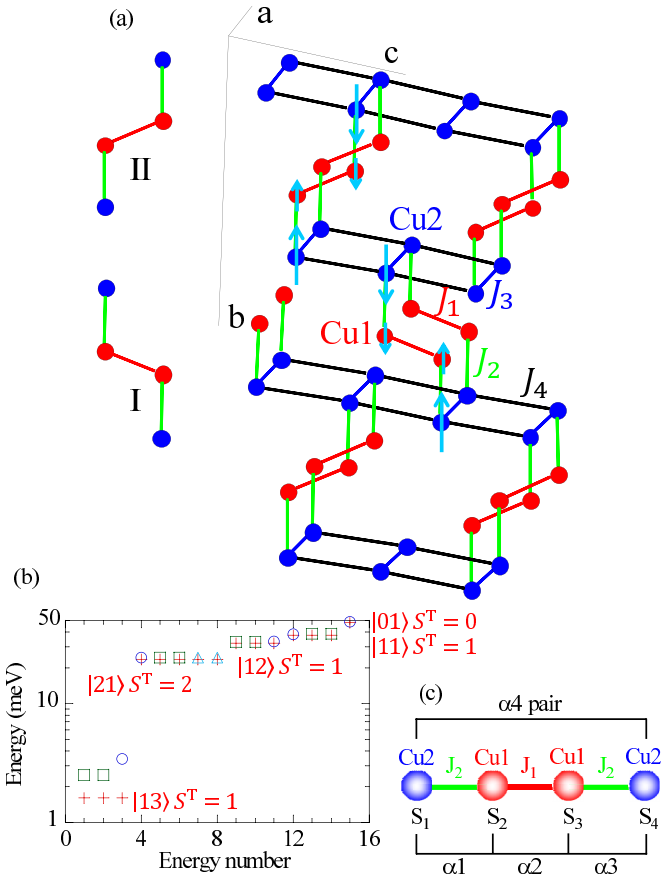

FIG. 1. (Color online) (a) Schematic drawing of Cu^{2+} ion positions having spin-$\frac{1}{2}$ in $Cu_2CdB_2O_6$. Two crystallographic Cu sites (Cu1 and Cu2) exist. Red and blue circles represent Cu1 and Cu2 sites, respectively. The J_1 and J_2 exchange interactions form spin tetramers. Two kinds of tetramers (I and II) exist, although the two are equivalent to each other as a spin system. We take the J_3 and J_4 intertetramer interactions into account. Arrows indicate ordered magnetic moments below $T_N = 9.8$ K. The space group is monoclinic $P2_1/c$ (No. 14) [26]. The lattice constants at 15 K are $a = 3.4047(5)$ Å, $b = 15.140(2)$ Å, $c = 9.298(1)$ Å, and $\beta = 92.80(1)^\circ$ [27]. (b) Energies of excited states from the GS in the isolated spin tetramer formed by the J_1 and J_2 interactions (+ symbol) and those in the tetramer in the ordered state (other symbols). We evaluated the exchange interaction parameters that reproduce the magnetic excitations observed by inelastic neutron scattering measurements. Their values are listed in Table I. S^T is the value of the sum of the spin operators in the tetramer. The eigenstates $|ij\rangle$ of the isolated tetramer are explicitly given in Ref. [30]. In the isolated tetramer, the GS is the spin-singlet $|02\rangle$ state. Circles, squares, and triangles indicate states with $S_z^T = 0, 1$, and 2, respectively, in the ordered state. (c) An illustration of the isolated tetramer to explain the $|02\rangle$ and $|13\rangle$ states. Details are described in the Appendix.

99%. We confirmed the formation of $Cu_2CdB_2O_6$ using an x-ray diffractometer (RINT-TTR III; Rigaku). We performed INS measurements using the disk-chopper-type spectrometer (AMATERAS) at BL 14 [28] in the Materials and Life Science Experimental Facility (MLF) of Japan Proton Accelerator Research Complex (J-PARC). We placed about 9 g of the powder in a vanadium cylinder with a diameter of 10 mm and mounted the cylinder in a ^{4}He closed cycle refrigerator. The

experimental data were obtained by the UTSUSEMI software provided by MLF [29].

We considered the model shown in Fig. 1(a). The J_1 and J_2 interactions are intratetramer interactions. The J_3 and J_4 interactions are intertetramer interactions. From the magnetic structure of $Cu_2CdB_2O_6$ [27], the J_1 and J_4 interactions are antiferromagnetic and the J_2 and J_3 interactions are ferromagnetic. The ordered moments in the calculation are parallel to the corresponding ordered moments determined experimentally. The moments are nearly parallel to the b axis. We calculated energies of ground and excited states of an isolated tetramer and a tetramer in the ordered state using the exact diagonalization [30] and tetramer mean-field theory, respectively [10]. We calculated the dispersion relation of magnetic excitations and the neutron scattering intensities of the model for $Cu_2CdB_2O_6$ shown in Fig. 1(a) using extended Holstein-Primakoff theory [10].

III. EXPERIMENTAL RESULTS

Figure 2 shows INS intensity $I(Q,\omega)$ maps of the $Cu_2{}^{114}Cd^{11}B_2O_6$ powder. Here, Q and ω are the magnitude of the scattering vector and the energy transfer, respectively. The energy of incident neutrons E_i is 7.74 meV. Excitations at 5.3 K are most apparent around $\omega = 2.3$ meV and $Q = 0.5$ Å^{-1}. The intensity of excitations between 1.7 and 2.9 meV is suppressed at higher Q. As the temperature T is raised, the excitation energies are lowered and the intensity of the excitations is suppressed. These results mean that the observed excitations are dominated by those of magnetic origin. Weak excitations exist at $\omega \lesssim 1.5$ meV in the region $Q = 0.7$–0.8 Å^{-1} at 5.3 K. The intensity of the excitations increases with T. Weak excitations also exist at $\omega \gtrsim 3.0$ meV at 5.3 K.

Figure 3 shows the ω dependence of $\mathrm{Im}\chi(Q,\omega) \equiv I(Q,\omega) * (1 - e^{-\omega/k_BT})$ for the $Cu_2{}^{114}Cd^{11}B_2O_6$ powder. As shown in Fig. 4 later, the Q dependence of the INS intensity has a maximum around $Q = 0.50$ and 0.55 Å^{-1} below and above $T_N = 9.8$ K, respectively. Therefore, Figs. 3(a) and 3(b) show $\mathrm{Im}\chi(Q,\omega)$ summed in the Q ranges of 0.40–0.60 and 0.45–0.65 Å^{-1} below 9.0 and above 9.9 K, respectively. $\mathrm{Im}\chi(Q,\omega)$ at 5.3 K shows a broad maximum whose center is at 2.3 meV. The horizontal bar indicates the energy resolution at $\omega = 0$ meV. $\mathrm{Im}\chi(Q,\omega)$ at 5.3 K is broader than the energy resolution. As the temperature T is raised, both the peak position as shown in the inset of Fig. 3(b) and the peak height are lowered. $\mathrm{Im}\chi(Q,\omega)$ at ω below the peak energy increases with T up to 12.5 K. $\mathrm{Im}\chi(Q,\omega)$ below 3.7 meV decreases with increasing T above 12.5 K. Figure 3(c) shows $\mathrm{Im}\chi(Q,\omega)$ summed in the Q range of 1.05–1.15 Å^{-1} at 5.3 K. We can see a maximum around 2.5 meV. As explained later, we used the excitation energy to evaluate the J_3 value.

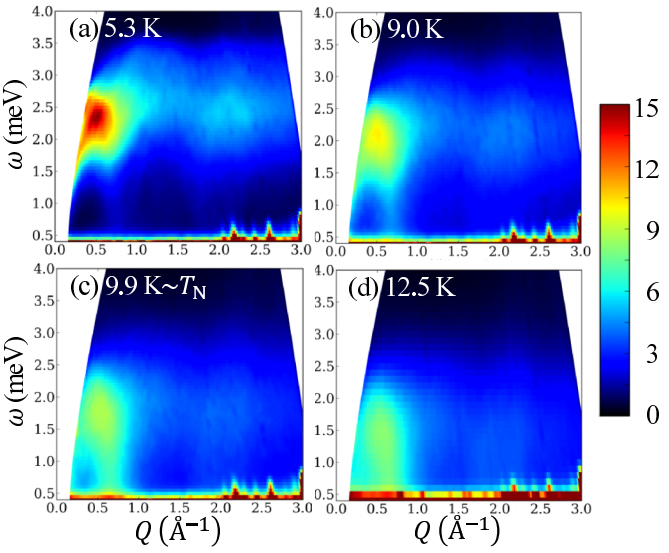

FIG. 2. (Color online) INS intensity $I(Q,\omega)$ maps in the $Q-\omega$ plane for the $Cu_2{}^{114}Cd^{11}B_2O_6$ powder at several temperatures. The energy of incident neutrons E_i is 7.74 meV. The right vertical key shows the INS intensity in arbitrary units.

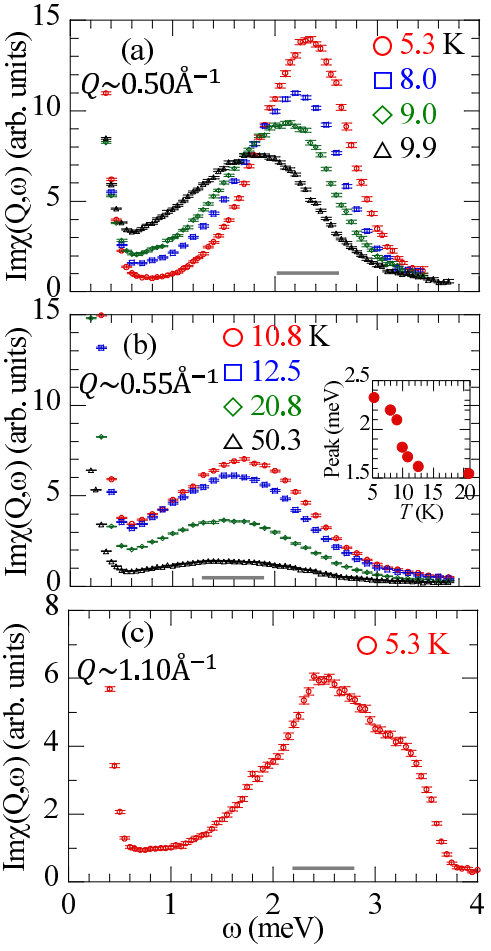

FIG. 3. (Color online) ω dependence of $\mathrm{Im}\chi(Q,\omega) \equiv I(Q,\omega) * (1 - e^{-\omega/k_BT})$ for the $Cu_2{}^{114}Cd^{11}B_2O_6$ powder. The energy of incident neutrons E_i is 7.74 meV. The horizontal bar indicates the energy resolution of 0.6 meV at $\omega = 0$ meV. (a) $\mathrm{Im}\chi(Q,\omega)$ summed in the Q range of 0.40–0.60 Å^{-1} at $T \leqslant 9.0$ K and 0.45–0.65 Å^{-1} at 9.9 K. (b) $\mathrm{Im}\chi(Q,\omega)$ summed in the Q range of 0.45–0.65 Å^{-1} at $T \geqslant 10.8$ K. The inset shows the T dependence of the peak energy of $\mathrm{Im}\chi(Q,\omega)$. (c) $\mathrm{Im}\chi(Q,\omega)$ summed in the Q range of 1.05–1.15 Å^{-1} at 5.3 K.

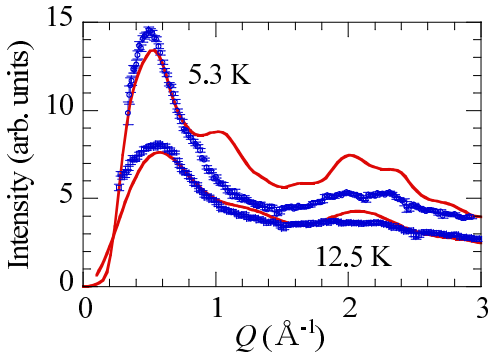

FIG. 4. (Color online) Q dependence of the INS intensity for the $Cu_2{}^{114}Cd^{11}B_2O_6$ powder. The energy of incident neutrons E_i is 7.74 meV. The data show the INS intensity summed in the ω range of 2.20–2.40 meV (1.25–1.65 meV) at 5.3 K (12.5 K). The two lines indicate the calculated results described in the text.

Figure 4 shows the Q dependence of the INS intensity around the peak of the magnetic excitations in Fig. 3. The intensities were summed in the ω ranges of 2.20–2.40 and 1.25–1.65 meV at 5.3 and 12.5 K, respectively. The intensity at 5.3 K in the ordered state shows broad peaks around $Q = 0.50$ and 2.10 Å^{-1}. The intensity at 12.5 K in the paramagnetic state shows broad peaks around $Q = 0.55$ and 2.10 Å^{-1} and a shoulder around $Q = 1.20$ Å^{-1}. We will explain the calculated lines later.

Magnetic excitations with higher energies exist. Figure 5 shows the ω dependence of the INS intensity summed in the Q range of 1.8–2.2 Å^{-1} for the $Cu_2{}^{114}Cd^{11}B_2O_6$ powder. The energy of incident neutrons E_i is 42.1 meV. Excitations can be seen at approximately 24 meV below $T_N = 9.8$ K. As T is raised, the intensities around 24 meV decrease. Therefore, magnetic excitations exist around 24 meV. Excitations can be observed at approximately 22 meV above T_N. As described later, we consider that magnetic excitations exist around 22 meV above T_N. In addition to the magnetic excitations, other excitations can be seen in the energy range shown in Fig. 5. From the T dependence, we consider that the other excitations are phonons.

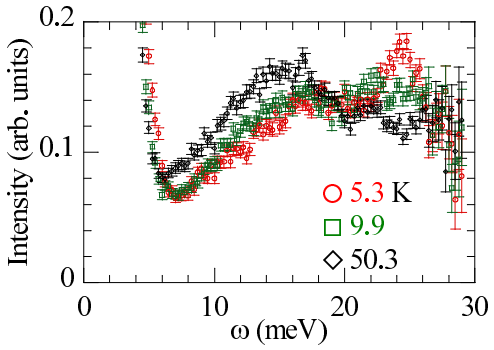

FIG. 5. (Color online) ω dependence of the INS intensity for the $Cu_2{}^{114}Cd^{11}B_2O_6$ powder. The energy of incident neutrons E_i is 42.1 meV. The data show the intensity summed in the Q range of 1.8–2.2 Å^{-1}. Red circles, green squares, and black diamonds show the data at 5.3, 9.9, and 50.3 K, respectively.

TABLE I. Values of exchange interaction parameters (in the units of meV) obtained in this study. We used the central values for calculations of the energies in Fig. 1(b), magnetic excitations in Figs. 4, 6(a), and 7(b).

J_1	J_2	J_3	J_4
27.3 ± 1.0	-14.0 ± 1.4	-0.4 ± 0.2	1.4 ± 0.2

IV. COMPARISON BETWEEN EXPERIMENTAL AND CALCULATED RESULTS

The values of the exchange interactions were evaluated as follows to explain the experimental results and are listed in Table I. We used the peak energies 1.6 meV above T_N and 24 meV at 5.3 K to evaluate the J_1 and J_2 values. As described later, the intertetramer J_3 and J_4 interactions are less relevant above T_N. The peak energy 1.6 meV is the energy difference of the GS and the first excited states (ESs) of the isolated tetramer. The peak energy 24 meV corresponds to the energy difference of the GS and the ESs with $S^T = 2$. In the ordered state at $T < T_N$, the $|13\rangle$ state participating in the GS enables the excitation. The energy difference is nearly independent of the J_3 and J_4 values. We evaluated $J_1 = 27.3 \pm 1.0$ and $J_2 = -14.0 \pm 1.4$ meV. We assumed that errors of the peak energies 1.6 and 24 meV were 0.2 and 1.0 meV, respectively, and estimated the errors of the J_1 and J_2 values. As described later, the strong intensities around $\omega = 2.3$ meV and $Q = 0.5$ Å^{-1} are generated by the excitations of the T_0 mode around (010) ($Q = 0.42$ Å^{-1}). The energy of the T_0 mode depends strongly on the J_4 value when the J_1 and J_2 values are fixed. We evaluated $J_4 = 1.4 \pm 0.2$ meV. We assumed that the error of the T_0 mode energy was 0.2 meV and estimated the error of the J_4 value. As shown in Fig. 3(c), $\mathrm{Im}\chi(Q,\omega)$ at 5.3 K around $Q = 1.1$ Å^{-1} shows the maximum at 2.5 meV. The excitation energy depends strongly on the J_3 value when the J_1 and J_2 values are fixed. We evaluated $J_3 = -0.4 \pm 0.2$ meV. We assumed that the error of the excitation energy was 0.2 meV and estimated the error of the J_3 value. We confirmed that AF-LRO appeared in the spin model with evaluated values including the errors of the exchange interactions.

Figure 1(b) shows the energies of the excited states of the tetramer [10,30]. In the isolated tetramer, the GS is the spin-singlet $|02\rangle$ state. The first excited states are the spin-triplet $|13\rangle$ states located at 1.6 meV. The next higher-energy excited states $|21\rangle$ are located at 23.6 meV. In the tetramer in the ordered state, the GS and excited states around 3 meV consist mainly of $|02\rangle$ and $|13\rangle$ states of the isolated tetramer. The excited states are located at 2.5, 3.4, and 24.3 meV, and higher energies.

Figure 6 shows the dispersion relations of the magnetic excitations and the neutron scattering intensities calculated at 0 K for the model of $Cu_2CdB_2O_6$ shown in Fig. 1. The appearance of the magnetic moment below T_N lifts the degeneracy and the triplet excitation splits into a doublet and a singlet. The former and the latter are accompanied by the transverse (T) and longitudinal (L) spin fluctuations of the ordered moment, respectively. They lead to the massless T modes (Nambu-Goldstone modes) and the massive L

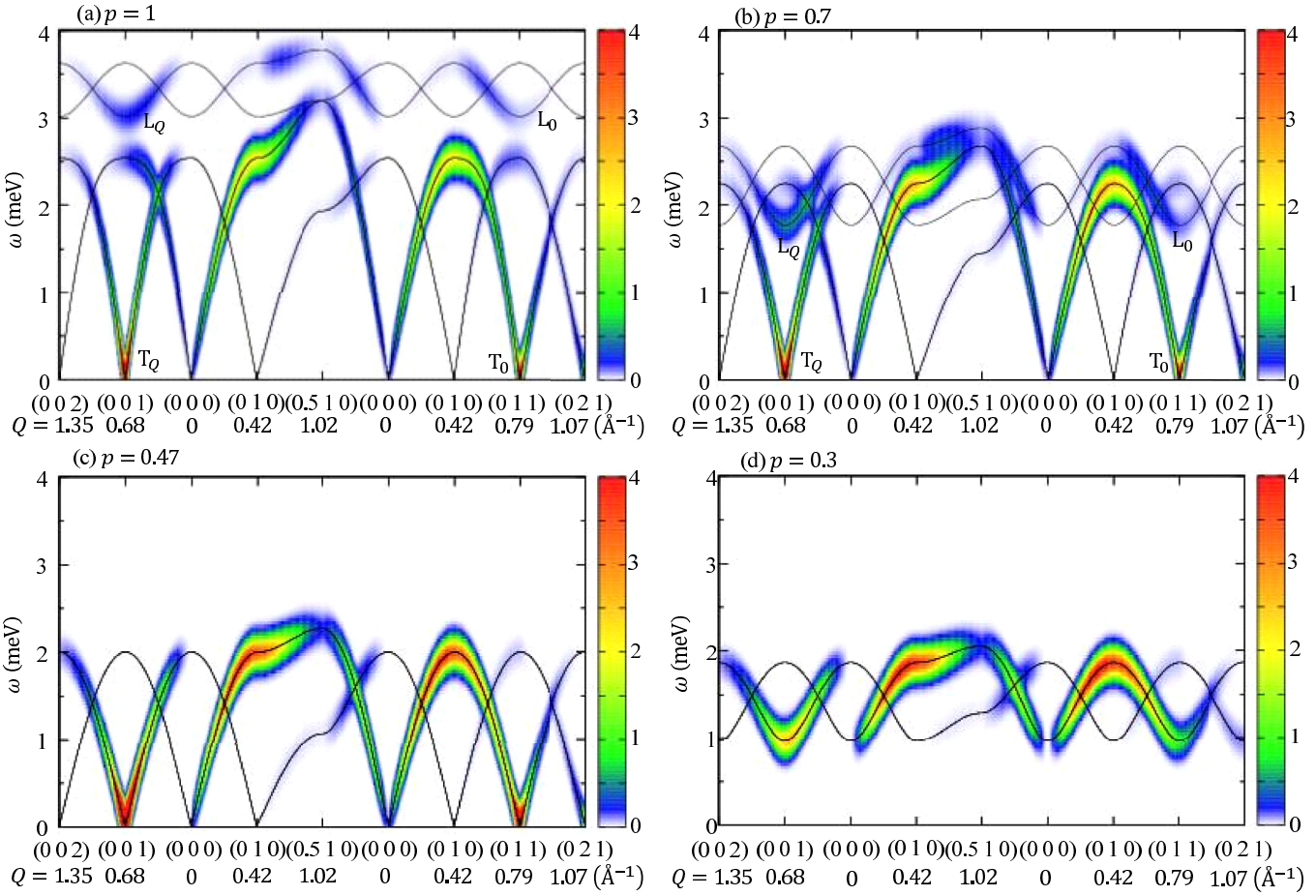

FIG. 6. (Color online) Dispersion relations of magnetic excitations (lines) along several symmetric axes calculated for the model of $Cu_2CdB_2O_6$ shown in Fig. 1 using extended Holstein-Primakoff theory. The neutron scattering intensities are also depicted. The values of the exchange interactions are $J_1 = 27.3$, $J_2 = -14.0$, $J_3 = -0.4p$, and $J_4 = 1.4p$ meV with $p = 1$, 0.7, 0.47, and 0.3 in (a), (b), (c), and (d), respectively. We used a broadening factor of $\Gamma = 0.5$ meV for the Gaussian function $\exp[-\frac{[\omega-\omega_d(\mathbf{Q})]^2}{\Gamma^2}]$, where $\omega_d(\mathbf{Q})$ is the excitation energy at $\mathbf{Q}$. In the ordered states (a) and (b), there are two transverse branches depicted as T_0 and T_Q, reflecting the two (I and II) tetramers in a unit cell, both of which are doubly degenerate. There are two L modes, L_0 and L_Q. In the critical state (c), the L and T modes become degenerate. The two lines reflect the two tetramers. In the paramagnetic state (d), the spin gap exists.

mode (Higgs mode), respectively, after taking account of the dispersion relations caused by the intertetramer interactions. Each mode has two branches denoted by the subscripts "0" and "Q" (T_0, T_Q, L_0, and L_Q), reflecting the two (I and II) tetramers in a unit cell.

Figures 7(a) and 7(b) show the INS intensity map for the $Cu_2{}^{114}Cd^{11}B_2O_6$ powder at 5.3 K and that calculated for the model of $Cu_2CdB_2O_6$ shown in Fig. 1, respectively, in the $Q-\omega$ plane. The two maps are similar to each other. The intensities in both figures are strong around $\omega = 2.3$ meV and $Q = 0.5$ Å^{-1}. The intensities are generated by the excitations of the T_0 mode around (010) ($Q = 0.42$ Å^{-1}). The weak excitations at $\omega \lesssim 1.5$ meV around $Q = 0.7$–0.8 Å^{-1} are caused by the branch from (011) ($Q = 0.79$ Å^{-1}) of the T_0 mode and the branch from (001) ($Q = 0.68$ Å^{-1}) of the T_Q mode. These are the gapless Nambu-Goldstone modes that appear because of the magnetic order. The weak excitations at $\omega \gtrsim 3$ meV are caused by the excitations of the T_0 mode around (0.510) ($Q = 1.02$ Å^{-1}) and L mode. The Higgs mode (L mode) may appear in $Cu_2CdB_2O_6$ at ambient pressure and zero magnetic field. The spin gap was calculated to be 1.6 meV in the isolated tetramer with $J_1 = 27.3$ meV and $J_2 = -14.0$ meV. Consequently, we were able to confirm that the spin gap was less than the effective intertetramer interaction value ($-2J_3 + 2J_4 = 3.6 \pm 0.8$ meV).

We next compare the experimental and calculated Q dependence of the intensity in Fig. 4. The upper line indicates the intensity of the excitation calculated for the model of $Cu_2CdB_2O_6$ shown in Fig. 1. The calculated intensities between 2.2 and 2.4 meV were summed. Although the intensities observed at 5.3 K are inconsistent with the upper line and the peak around $Q = 1.1$ Å^{-1} was not observed experimentally, the line is similar to the INS intensity at 5.3 K. The lower line indicates the intensity of the excitation from the spin-singlet GS to the spin-triplet first excited states in the isolated spin tetramer with $J_2/J_1 = -0.51$. The line is close to the INS intensity at 12.5 K in the paramagnetic state. The peak position around $Q = 0.5$ Å^{-1} is slightly lower in the data at 5.3 K and upper line than in the data at 12.5 K and lower line, respectively.

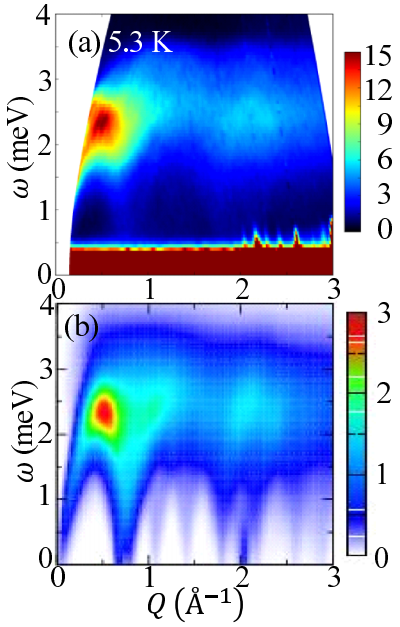

FIG. 7. (Color online) (a) INS intensity $I(Q,\omega)$ map in the $Q-\omega$ plane for the $Cu_2{}^{114}Cd^{11}B_2O_6$ powder at 5.3 K. The energy of incident neutrons E_i is 7.74 meV. The right vertical key shows the intensity in arbitrary units. (b) INS intensity map in the $Q-\omega$ plane calculated for the model of $Cu_2CdB_2O_6$ shown in Fig. 1 using extended Holstein-Primakoff theory. The values of the exchange interactions are listed in Table I. We used a broadening factor of $\Gamma = 0.5$ meV.

The width of the peak around $Q = 0.5$ Å^{-1} is slightly narrower in the data at 5.3 K and upper line than in the data at 12.5 K and lower line, respectively. The slight changes of the peak position and width suggest that the J_3 and J_4 interactions are relevant in the ordered state.

V. DISCUSSION

First, we consider the effects of temperature. In the spin dimer system $TlCuCl_3$, the thermally populated triplet excitations block their movement. This leads to the suppression of the effective interdimer interactions by increasing T [19,20]. In $Cu_2CdB_2O_6$, the values of the intertetramer interactions ($J_3 = -0.4 \pm 0.2$ and $J_4 = 1.4 \pm 0.2$ meV) are comparable to or lower than the temperatures at which the data in Fig. 3 were obtained. The intertetramer interactions are less relevant at higher T in the T range in Fig. 3. Each tetramer is affected by internal magnetic fields generated by magnetic moments on neighboring tetramers. As T is raised, the magnitudes of the magnetic moments decrease and the effect of internal magnetic fields decreases. Accordingly, the excitation energies in weakly coupled tetramers decrease and approach those in the isolated tetramers.

To investigate the effects of temperature, we calculated dispersion relations of the magnetic excitations at 0 K for $J_1 = 27.3$, $J_2 = -14.0$, $J_3 = -0.4p$, and $J_4 = 1.4p$ meV with $p \leqslant 1$. Figure 6 shows the calculated results. The energy range where the magnetic excitations of the T modes exist decreases with p. The excitations around $Q = 0.5$ Å^{-1} in the experimental results are caused by the T_0 mode around (010). The T_0 mode energy at (010) decreases with p. The magnetic excitations of the L_0 mode around (011) and the L_Q mode around (001) shift to markedly lower energies with decreasing p. The excitation gap of the L mode at (011) and (001) decreases accordingly and vanishes at the critical value $p = 0.47$ that corresponds to T_N. The L and T modes become degenerate at $p = 0.47$. No ordered magnetic moment exists at $p = 0.3$. Excitations are gapped because of the paramagnetic state. The band width is narrower with decreasing p.

The p dependence is similar to the T dependence of the experimental results. As T is raised, the peak energy shifts to lower energy as shown in the inset of Fig. 3(b) and the intensity between 0.5 and 1.7 meV in Fig. 3(a) increases at $T < T_N$. Probably, we observed experimentally the suppression of the effective interdimer interactions by increasing T, although we could not prove experimentally the decrease of the band width with increasing T at $T > T_N$.

The intertetramer interactions also exist at $T > T_N$ and generate excitation bands with finite widths as in the case that $p = 0.3$. The excitations from thermally excited states in each band probably generated the continuous low-energy intensities in Fig. 3. In addition, as described in the Introduction, the GS is magnetic because of the intertetramer interactions. Paramagnetic scattering from the GS may also contribute to the intensities at low ω. Consequently, at $T > T_N$, it is difficult to observe a clear excitation gap with powder samples, although the magnetic excitations are expected to be gapped because of the absence of gapless Nambu-Goldstone modes.

The high-energy magnetic excitations in Fig. 5 can also be explained by the spin tetramers. At $T > T_N$, the excitations around 22 meV correspond to those between the $|13\rangle(S^T = 1)$ and $|21\rangle(S^T = 2)$ states, which have an energy difference of 22.0 meV in the isolated spin tetramer. Note that the excitation from the GS $|02\rangle(S^T = 0)$ to the $|21\rangle(S^T = 2)$ (23.6 meV) state is forbidden in the isolated spin tetramer. In the ordered state at $T < T_N$, the excitations around 24 meV correspond to those from the ground state to the excited states located at 24.3 meV as shown in Fig. 1(b). In this case, the $|13\rangle$ state participating in the GS enables the excitations.

The origin of the $\frac{1}{2}$ quantum magnetization plateau is essentially the energy difference between the $|13\rangle(S^T = 1)$ and $|21\rangle(S^T = 2)$ states. The latter state cannot contribute to the magnetization because of the energy difference. The magnetization cannot increase from $S_z^T = 1$ and the $\frac{1}{2}$ quantum magnetization plateau continues until one of $|21\rangle$ states with $S_z^T = 2$ is stabilized by the magnetic field. We calculated the magnetization curve at 0 K using the extended Holstein-Primakoff (EHP) theory and that at 2.9 K using a quantum Monte Carlo (QMC) technique (not shown). The $\frac{1}{2}$ magnetization plateau appears above $H_p = 33$, 42, and 23 T in the EHP, QMC, and experimental results, respectively. We could not find J values which could explain both the INS and magnetization results. The H_p value depends strongly on the J_4 interaction. We expect that both the INS and magnetization results can be reproduced by calculated results including other weak intertetramer interactions. To solve the discrepancy between the H_p values, we need more precise information on exchange interactions that may be obtained in INS experiments using single crystals of $Cu_2CdB_2O_6$. We will

be able to confirm experimentally the existence of the Higgs mode in INS experiments using single crystals.

The magnetic excitations around 24 meV in Fig. 5 indicate that the character of the spin cluster (energy gap) remains even in the ordered state. This is probably a common feature of spin clusters. As described earlier, in $Cu_2Fe_2Ge_4O_{13}$, magnetic excitations around 24 meV generated by Cu dimers were observed below T_N [8]. The spin system of $Cu_3Mo_2O_9$ consists of AF chains and dimers [31,32]. Magnetic excitations around 6 meV mainly generated by the dimers were observed below T_N [33,34]. AF-LRO appears upon the substitution of other ions for Cu or Ge sites in the spin-Peierls substance $CuGeO_3$ [2–4]. Magnetic excitations originating from the singlet-triplet excitation of dimers remain below T_N [35]. In the spinel antiferromagnets $ZnCr_2O_4$ and $MgCr_2O_4$, quasielastic scattering in the paramagnetic state can be explained by the spin-molecule (hexamer) model [36,37], where the spin molecules are generated by geometrical frustration. Two modes appear at 4.5 and 9.0 meV in the ordered state and can be explained by hexamers and heptamers, respectively [37]. The spin molecules are interpreted to be quasiparticles of highly frustrated spins.

Finally, we comment on another spin model for $Cu_2CdB_2O_6$ proposed in Ref. [38]. By performing extensive density functional theory band-structure calculations, four dominant exchange interactions were identified. The four exchange interactions form a frustrated quasi-two-dimensional magnetic model. This spin model accounts for the magnetization results. It is important to investigate theoretically whether the spin model can also explain the magnetic excitations observed in our study.

VI. CONCLUSION

We performed inelastic neutron scattering experiments on $Cu_2{}^{114}Cd^{11}B_2O_6$ powder. The magnetic excitations at low temperatures are similar to those of the spin-$\frac{1}{2}$ tetramers in the ordered state. The weak excitations at $\omega \gtrsim 3$ meV suggest that the Higgs mode (L mode) appears in $Cu_2CdB_2O_6$ at ambient pressure and zero magnetic field. We evaluated $J_1 = 27.3 \pm 1.0$ and $J_2 = -14.0 \pm 1.4$ meV for the intratetramer interactions and $J_3 = -0.4 \pm 0.2$ and $J_4 = 1.4 \pm 0.2$ meV for the intertetramer interactions. With these exchange interaction parameters, the low-energy excitations of $Cu_2CdB_2O_6$ are dominated by the singlet-triplet states of a tetramer. This means that the low-energy physics can be described by an interacting spin-dimer (singlet-triplet) system. The spin gap in the isolated spin tetramer was calculated to be 1.6 meV, which is less than the effective intertetramer interaction value (3.6 ± 0.8 meV). Therefore, antiferromagnetic long-range order is possible, although the ground state of the isolated spin tetramer is the spin-singlet state. As the temperature T) is raised, the magnetic excitations shift to lower energies and the intensities at low energies increase. The temperature dependencies can be understood as resulting from the less relevant intertetramer interactions at higher T, the decrease of the magnetic moments, and the decrease of the excitation energies of the longitudinal mode (Higgs mode) around the gapless points. Consequently, as T is raised, the excitation energies in weakly coupled tetramers approach those in the isolated tetramers. The spin gap in the isolated spin tetramer (1.6 meV) is close to the peak position of the magnetic excitations above T_N.

ACKNOWLEDGMENTS

This work was financially supported by Japan Society for the Promotion of Science (JSPS) KAKENHI (Grant No. 23540396) and grants from National Institute for Materials Science (NIMS). M.M. was supported by KAKENHI (Grant No. 26400332). The neutron scattering experiments were approved by the Neutron Science Proposal Review Committee of Japan Proton Accelerator Research Complex (J-PARC) Materials and Life Science Experimental Facility (MLF) (Proposal No. 2013A0008) and supported by the Inter-University Research Program on Neutron Scattering of Institute of Materials Structure Science (IMSS), High Energy Accelerator Research Organization (KEK). We are grateful to M. Kohno, T. Masuda, H. Kuroe, and K. Tomiyasu for fruitful discussions and to S. Matsumoto for sample syntheses and x-ray diffraction measurements.

APPENDIX: |02⟩ AND |13⟩ STATES

We explain the $|02\rangle$ and $|13\rangle$ states of the isolated tetramer using Fig. 1(c). We designate a spin pair formed by S_j and S_{j+1} as an α_j pair. The $|02\rangle$ state is expressed as $C_{01}(|\downarrow\downarrow\uparrow\uparrow\rangle + |\uparrow\uparrow\downarrow\downarrow\rangle - |\downarrow\uparrow\downarrow\uparrow\rangle - |\uparrow\downarrow\uparrow\downarrow\rangle) + C_{02}(|\downarrow\uparrow\downarrow\uparrow\rangle + |\uparrow\downarrow\uparrow\downarrow\rangle - |\uparrow\downarrow\downarrow\uparrow\rangle - |\downarrow\uparrow\uparrow\downarrow\rangle) = C_{01}(|\downarrow\uparrow\rangle - |\uparrow\downarrow\rangle)_{\alpha 2} * (|\downarrow\uparrow\rangle - |\uparrow\downarrow\rangle)_{\alpha 4} + C_{02}(|\downarrow\uparrow\rangle - |\uparrow\downarrow\rangle)_{\alpha 1} * (|\downarrow\uparrow\rangle - |\uparrow\downarrow\rangle)_{\alpha 3}$. The symbols $\uparrow$ and $\downarrow$ in kets $|\ldots\rangle$ means $S_{jz} = \frac{1}{2}$ and $-\frac{1}{2}$ ($j = 1$ to 4), respectively. For example, $|\downarrow\downarrow\uparrow\uparrow\rangle$ means $|S_{1z} = -\frac{1}{2}, S_{2z} = -\frac{1}{2}, S_{3z} = \frac{1}{2}, S_{4z} = \frac{1}{2}\rangle$. The first term is a product of a singlet state in the α_2 pair and a singlet state in the α_4 pair. The second term is a product of a singlet state in the α_1 pair and a singlet state in the α_3 pair. The two coefficients are $C_{01} = \frac{1}{\sqrt{3+(-1+4j+2\sqrt{1-2j+4j^2})^2}}$ and $C_{02} = \frac{2-4j-2\sqrt{1-2j+4j^2}}{2\sqrt{3+(-1+4j+2\sqrt{1-2j+4j^2})^2}}$. The $|13\rangle$ state with $S_z^{\mathrm{T}} = 1$ is expressed as $C_{11}(|\uparrow\downarrow\uparrow\uparrow\rangle - |\uparrow\uparrow\downarrow\uparrow\rangle) + C_{12}(|\downarrow\uparrow\uparrow\uparrow\rangle - |\uparrow\uparrow\uparrow\downarrow\rangle) = C_{11}(|\downarrow\uparrow\rangle - |\uparrow\downarrow\rangle)_{\alpha 2} * |\uparrow\uparrow\rangle_{\alpha 4} + C_{12}(|\downarrow\uparrow\rangle - |\uparrow\downarrow\rangle)_{\alpha 4} * |\uparrow\uparrow\rangle_{\alpha 2}$. The first term is a product of a singlet state in the α_2 pair and a triplet state with $S_z = 1$ in the α_4 pair. The second term is a product of a singlet state in the α_4 pair and a triplet state with $S_z = 1$ in the α_2 pair. The two coefficients are $C_{11} = \frac{1+j+\sqrt{1+j^2}}{2\sqrt{1+(j+\sqrt{1+j^2})^2}}$ and $C_{12} = \frac{1-j-\sqrt{1+j^2}}{2\sqrt{1+(j+\sqrt{1+j^2})^2}}$.

[1] P. W. Anderson, The resonating valence bond state in La_2CuO_4 and superconductivity, Science **235**, 1196 (1987).

[2] M. Hase, I. Terasaki, and K. Uchinokura, Observation of the Spin-Peierls Transition in Linear Cu^{2+} (Spin-$\frac{1}{2}$) Chains in an Inorganic Compound $CuGeO_3$, Phys. Rev. Lett. **70**, 3651 (1993).

[3] M. Hase, I. Terasaki, Y. Sasago, K. Uchinokura, and H. Obara, Effects of Substitution of Zn for Cu in the Spin-Peierls Cuprate, $CuGeO_3$: The Suppression of the Spin-Peierls Transition and the Occurrence of a New Spin-Glass State, Phys. Rev. Lett. **71**, 4059 (1993).

[4] M. Hase, I. Terasaki, K. Uchinokura, M. Tokunaga, N. Miura, and H. Obara, Magnetic phase diagram of the spin-Peierls cuprate $CuGeO_3$, Phys. Rev. B **48**, 9616 (1993).

[5] F. D. M. Haldane, Spontaneous dimerization in the $S = \frac{1}{2}$ Heisenberg antiferromagnetic chain with competing interactions, Phys. Rev. B **25**, 4925(R) (1982).

[6] F. D. M. Haldane, Erratum: Spontaneous dimerization in the $S = \frac{1}{2}$ Heisenberg antiferromagnetic chain with competing interactions, Phys. Rev. B **26**, 5257 (1982).

[7] K. Okamoto and K. Nomura, Fluid-dimer critical point in $S = 1/2$ antiferromagnetic Heisenberg chain with next nearest neighbor interactions, Phys. Lett. A **169**, 433 (1992).

[8] T. Masuda, K. Kakurai, and A. Zheludev, Spin dimers in the quantum ferrimagnet $Cu_2Fe_2Ge_4O_{13}$ under staggered and random magnetic fields, Phys. Rev. B **80**, 180412(R) (2009).

[9] J. Goldstone, A. Salam, and S. Weinberg, Broken symmetries, Phys. Rev. **127**, 965 (1962).

[10] M. Matsumoto, H. Kuroe, T. Sekine, and T. Masuda, Transverse and longitudinal excitation modes in interacting multispin systems, J. Phys. Soc. Jpn. **79**, 084703 (2010).

[11] B. Kurniawan, M. Ishikawa, T. Kato, H. Tanaka, K. Takizawa, and T. Goto, Novel three-dimensional magnetic ordering in the quantum spin system NH_4CuCl_3, J. Phys.: Condens. Matter **11**, 9073 (1999).

[12] K. Goto, M. Fujisawa, H. Tanaka, Y. Uwatoko, A. Oosawa, T. Osakabe, and K. Kakurai, Pressure-induced magnetic quantum phase transition in gapped spin system $KCuCl_3$, J. Phys. Soc. Jpn. **75**, 064703 (2006).

[13] H. Tanaka, K. Goto, M. Fujisawa, T. Ono, and Y. Uwatoko, Magnetic ordering under high pressure in the quantum spin system $TlCuCl_3$, Physica B (Amsterdam) **329–333**, 697 (2003).

[14] M. Matsumoto, Microscopic model for the magnetization plateaus in NH_4CuCl_3, Phys. Rev. B **68**, 180403(R) (2003).

[15] Ch. Rüegg, M. Oettli, J. Schefer, O. Zaharko, A. Furrer, H. Tanaka, K. W. Krämer, H.-U. Güdel, P. Vorderwisch, K. Habicht, T. Polinski, and M. Meissner, Neutron Scattering Study of the Field-Dependent Ground State and the Spin Dynamics in Spin-One-Half NH_4CuCl_3, Phys. Rev. Lett. **93**, 037207 (2004).

[16] M. Matsumoto, Theoretical study of magnetic excitation in interacting inequivalent spin dimer system NH_4CuCl_3, J. Phys. Soc. Jpn. **84**, 034701 (2015).

[17] A. Oosawa, T. Ono, K. Kakurai, and H. Tanaka, Magnetic excitations in the quantum spin system NH_4CuCl_3, arXiv:cond-mat/0304172.

[18] M. Matsumoto, B. Normand, T. M. Rice, and M. Sigrist, Field- and pressure-induced magnetic quantum phase transitions in $TlCuCl_3$, Phys. Rev. B **69**, 054423 (2004).

[19] Ch. Rüegg, B. Normand, M. Matsumoto, A. Furrer, D. F. McMorrow, K. W. Krämer, H.-U. Güdel, S. N. Gvasaliya, H. Mutka, and M. Boehm, Quantum Magnets under Pressure: Controlling Elementary Excitations in $TlCuCl_3$, Phys. Rev. Lett. **100**, 205701 (2008).

[20] P. Merchant, B. Normand, K. W. Krämer, M. Boehm, D. F. McMorrow, and Ch. Rüegg, Quantum and classical criticality in a dimerized quantum antiferromagnet, Nat. Phys. **10**, 373 (2014).

[21] T. Masuda, B. C. Chakoumakos, C. L. Nygren, S. Imai, and K. Uchinokura, A novel germanate, $Cu_2Fe_2Ge_4O_{13}$, with a four tetrahedra oligomer, J. Solid State Chem. **176**, 175 (2003).

[22] T. Masuda, A. Zheludev, B. Grenier, S. Imai, K. Uchinokura, E. Ressouche, and S. Park, Cooperative Ordering of Gapped and Gapless Spin Networks in $Cu_2Fe_2Ge_4O_{13}$, Phys. Rev. Lett. **93**, 077202 (2004).

[23] T. Masuda, A. Zheludev, B. Sales, S. Imai, K. Uchinokura, and S. Park, Magnetic excitations in the weakly coupled spin dimers and chains material $Cu_2Fe_2Ge_4O_{13}$, Phys. Rev. B **72**, 094434 (2005).

[24] T. Masuda, K. Kakurai, M. Matsuda, K. Kaneko, and N. Metoki, Indirect magnetic interaction mediated by a spin dimer in $Cu_2Fe_2Ge_4O_{13}$, Phys. Rev. B **75**, 220401(R) (2007).

[25] M. Hase, M. Kohno, H. Kitazawa, O. Suzuki, K. Ozawa, G. Kido, M. Imai, and X. Hu, Coexistence of a nearly spin-singlet state and antiferromagnetic long-range order in quantum spin system $Cu_2CdB_2O_6$, Phys. Rev. B **72**, 172412 (2005).

[26] S. Münchau and K. Bluhm, Synthesis and crystal structure of coppcr cadmium pyroborate oxide: $Cu_2Cd(B_2O_5)O$, Z. Naturforsch. B: J. Chem. Sci. **50**, 1151 (1995).

[27] M. Hase, A. Dönni, V. Yu. Pomjakushin, L. Keller, F. Gozzo, A. Cervellino, and M. Kohno, Magnetic structure of $Cu_2CdB_2O_6$ exhibiting a quantum-mechanical magnetization plateau and classical antiferromagnetic long-range order, Phys. Rev. B **80**, 104405 (2009).

[28] K. Nakajima, S. Ohira-Kawamura, T. Kikuchi, M. Nakamura, R. Kajimoto, Y. Inamura, N. Takahashi, K. Aizawa, K. Suzuya, K. Shibata, T. Nakatani, K. Soyama, R. Maruyama, H. Tanaka, W. Kambara, T. Iwahashi, Y. Itoh, T. Osakabe, S. Wakimoto, K. Kakurai, F. Maekawa, M. Harada, K. Oikawa, R. E. Lechner, F. Mezei, and M. Arai, AMATERAS: A cold-neutron disk chopper spectrometer, J. Phys. Soc. Jpn. **80**, SB028 (2011).

[29] Y. Inamura, T. Nakatani, J. Suzuki, and T. Otomo, Development status of software utsusemi for chopper spectrometers at MLF, J-PARC, J. Phys. Soc. Jpn. **82**, SA031 (2013).

[30] M. Hase, K. M. S. Etheredge, S.-J. Hwu, K. Hirota, and G. Shirane, Spin-singlet ground state with energy gaps in Cu_2PO_4: Neutron-scattering, magnetic-susceptibility, and ESR measurements, Phys. Rev. B **56**, 3231 (1997). In this reference, the Hamiltonian is defined as $\mathcal{H} = \sum_{i,j} 2J_{ij} S_i \cdot S_j$ instead of $\mathcal{H} = \sum_{i,j} J_{ij} S_i \cdot S_j$ in this paper.

[31] T. Hamasaki, T. Ide, H. Kuroe, T. Sekine, M. Hase, I. Tsukada, and T. Sakakibara, Successive phase transitions to antiferromagnetic and weak-ferromagnetic long-range order in the quasi-one-dimensional antiferromagnet $Cu_3Mo_2O_9$, Phys. Rev. B **77**, 134419 (2008).

[32] M. Hase, H. Kitazawa, K. Ozawa, T. Hamasaki, H. Kuroe, and T. Sekine, Enhancement of magnetic frustration caused by Zn doping in quasi-one-dimensional quantum antiferromagnet $Cu_3Mo_2O_9$, J. Phys. Soc. Jpn. **77**, 034706 (2008).

[33] H. Kuroe, T. Hamasaki, T. Sekine, M. Hase, K. Oka, T. Ito, H. Eisaki, K. Kaneko, N. Metoki, M. Matsuda, and K. Kakurai, Hybridization of magnetic excitations between quasi-one-dimensional spin chains and spin dimers in $Cu_3Mo_2O_9$ observed using inelastic neutron scattering, Phys. Rev. B **83**, 184423 (2011).

[34] M. Matsumoto, H. Kuroe, T. Sekine, and M. Hase, Magnetic excitation and electric polarization in strongly coupled spin monomer and dimer system $Cu_3Mo_2O_9$, J. Phys. Soc. Jpn. **81**, 024711 (2012).

[35] M. C. Martin, M. Hase, K. Hirota, G. Shirane, Y. Sasago, N. Koide, and K. Uchinokura, Spin-Peierls and antiferromagnetic phases in $Cu_{1-x}Zn_xGeO_3$: A neutron-scattering study, Phys. Rev. B **56**, 3173 (1997).

[36] S.-H. Lee, C. Broholm, W. Ratcliff, G. Gasparovic, Q. Huang, T. H. Kim, and S.-W. Cheong, Emergent excitations in ageometrically frustrated magnet, Nature (London) **418**, 856 (2002).

[37] K. Tomiyasu, H. Suzuki, M. Toki, S. Itoh, M. Matsuura, N. Aso, and K. Yamada, Molecular Spin Resonance in the Geometrically Frustrated Magnet $MgCr_2O_4$ by Inelastic Neutron Scattering, Phys. Rev. Lett. **101**, 177401 (2008).

[38] O. Janson, I. Rousochatzakis, A. A. Tsirlin, J. Richter, Yu. Skourski, and H. Rosner, Decorated Shastry-Sutherland lattice in the spin-$\frac{1}{2}$ magnet $CdCu_2(BO_3)_2$, Phys. Rev. B **85**, 064404 (2012).